PROPERTIES AND APPLICATIONS FOR IRON POWDER MADE BY GAS ATOMIZATION

Kalathur Narasimhan
P2P Technologies
Moorestown, NJ 08057

Chris Schade, Kylan McQuaig and Carter Tesch
Hoeganaes Corporation
Cinnaminson, NJ

ABSTRACT

Applications and properties of iron powder made by inert gas atomization are reviewed. Iron powders are used in many different applications such as**:** soft magnetics, catalysts, water remediation, ink and toner carriers, coatings such as magnetic paints, welding, food grade iron for iron fortification, additives to dyes and stains. The gas atomization of pure iron is sometimes difficult due to the reaction of the iron with the refractories used in the introduction of the molten metal to the atomizing jet. The current process overcomes this limitation and the gas atomized iron powders in this study are reviewed in comparison to electrolytic iron in terms of particle size, shape, grain size and porosity levels. Applications of the iron, particularly, in terms of magnetic properties and use in 3D printing, are also reviewed.

INTRODUCTION

The applications for high purity iron powders have seen a significant increase in recent years due to the focus of the global community on energy and environment. With the recent shift to electric vehicles, use of high purity iron powder has grown in the areas of soft magnetic materials and as potential in battery applications.[1-3] Environmental applications include use in the field of water remediation and as catalysts in chemical reactions.[4-6] Soft magnetic properties are greatly influenced by the impurities. Permeability is the most important factor as it influences the amount of current required to achieve induction required in electromagnetic devices.

The focus in this publication is on powder metallurgical means to achieve pure iron and alloys of iron for use in additive manufacturing. The properties of the powders can vary with the production method to manufacture them, which include electrolytic, reduction of iron ore (sponge iron powder) and atomization. Each process leads to different properties (including shape, size distribution and purity), which leads to different applications in which they can be utilized. Figure 1 shows the typical morphology of iron powder produced by each manufacturing method. In relation to morphology, the sponge iron is generally considered the most irregular of the powders with the most internal porosity and lends itself to applications which surface area is the required feature. In regard to purity, sponge iron is reduced from iron ore and even after the reduction process can still contain significant levels of unreduced iron oxide and impurities such as SiO_2 and V_2O_5.

Most iron powders that are produced by atomization utilize water as the atomizing medium. In addition, due to the oxidation of the molten iron, the powders are generally annealed in hydrogen atmosphere to lower the overall bulk oxygen content of the powder as well as reduce any of the internal oxides that may

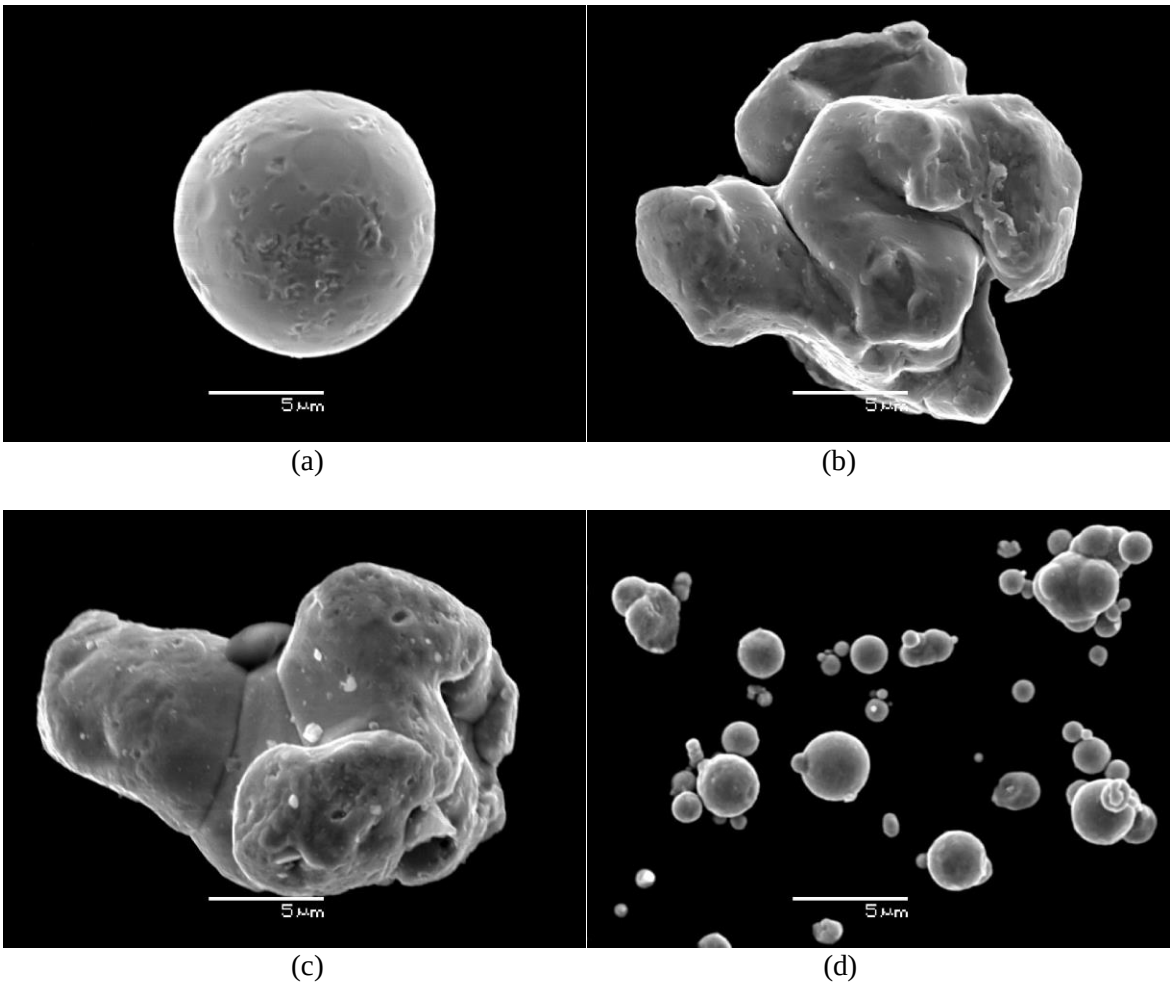

(a) (b)

(c) (d)

Figure 1: Morphology of typical sources of iron powder: (a) Gas Atomized, (b) Water Atomized, (c) Sponge Iron and (d) Carbonyl

get entrapped during the atomization process. The internal porosity of the water atomized powders is generally low and the powders produced by this process are very economical compared to their gas atomized counterpart. The most common use for water atomized iron powder is for automotive parts made by powder metallurgy utilizing compaction and sintering. The iron is produced by melting scrap iron from recycled materials including automotive parts, appliances, structural steel and everyday items. For this reason, water atomized iron powders are typically higher in residual elements such as copper, sulfur, chromium, nickel, phosphorus, etc. The steelmaking process used to produce these powders utilizes refractory materials, so some inclusions may also be present in the form of oxides. This lack of purity can limit the powders' use in applications where magnetic properties or conductivity are required. Producing fine iron powder (<25 microns) from typical water atomization is also difficult, as the higher surface area of the finer particles leads to higher oxygen, which is difficult to reduce in the hydrogen annealing process without agglomerating the fine material.

Fine iron powder can be made by the carbonyl process, which involves chemical decomposition of pentacarbonyl under pressure and temperature. The end result of the process is very fine iron powder, spherical in nature, with low elemental impurities such as chromium, sulfur, copper, nickel and phosphorus, but intermediate levels of carbon, oxygen and nitrogen. The high interparticle friction of the fine powder leads to a powder with poor flowability.

To satisfy the future and current requirements utilizing pure iron powders, a different manufacturing process than those described previously was established. The process entails using pure iron bar stock made by conventional steelmaking. The steelmaking process for the bar stock starts from high purity iron melted in a BOF (basic oxygen steelmaking furnace) and then further purified by ladle refining. The iron that is produced is low in residuals and the level of secondary inclusions is reduced by the refining of the metal. The molten metal is then continuous cast and rolled into bar stock that has its surface shot blasted to remove any oxidation. Typical chemistry of the iron bars is shown in Table I.

Table I: Iron Bar Chemistry

Material	Mn	Cr	Ni	P	Al	V	Cu	Al	Ti	C	Oxygen	Nitrogen
Iron Bar Stock	0.02	0.01	0.01	0.003	0.0005	0.001	0.01	0.0005	0.001	0.00	0.008	0.002

In order to convert the bar (typically one meter in length and 50-75 mm in diameter) into powder, a commercially accepted production route called the EIGA (Electrode Induction melting Gas Atomization) process is utilized.

The EIGA atomizer does not utilize a refractory crucible or nozzle, but instead the solid bar, while rotating, is fed into a small induction coil (Figure 2). The molten metal then drips from the bar into the atomizing jet without the use of any refractory material, thus minimizing any inclusions. The melting takes place under a protective argon atmosphere and the melt stream is atomized into powder using argon and collected in a container while keeping the material inert.

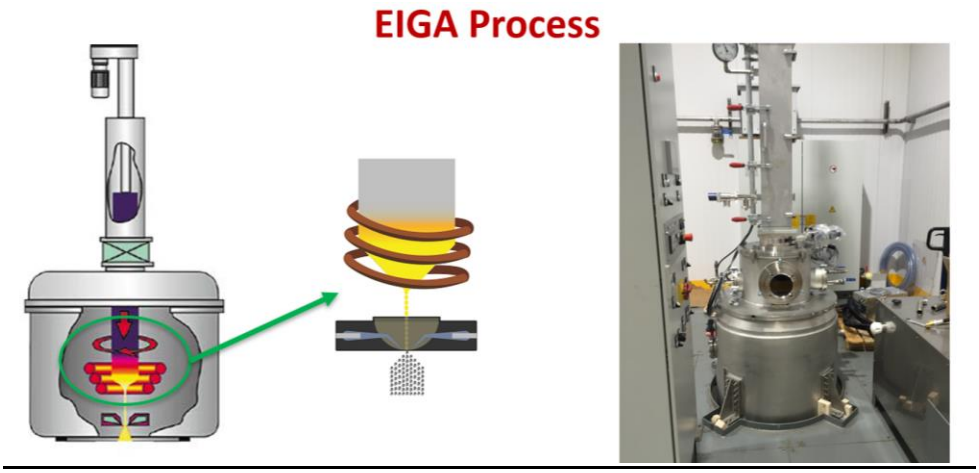

Figure 2: Depiction of Electrode Induction Melting Gas Atomization (EIGA). Note: EIGA is a trademark of ALD Vacuum Technologies.

EXPERIMENTAL PROCEDURE

In order to evaluate the EIGA processing route for pure iron powders, it was decided to compare the magnetic properties of the powder to that of more conventional processing routes. Magnetic properties of iron powders are directly related to the purity, grain size and oxygen content of the powder itself, lending it to be a good indication of the quality of the powder. Additionally, in order to evaluate the full powder size distribution produced by atomizing, it was decided to utilize additive manufacturing (AM) to produce

test specimens for evaluation. Three different AM manufacturing processes were utilized: Laser Powder Bed Fusion (LPBF), Metal Binder Jet (MBJ), and Direct Energy Deposition (DED). The LPBF process requires a powder in the 15–53-micron range, while the MBJ process requires a finer powder for sinterability, in the < 25-micron range. The DED process utilizes a 45-105 micron cut. These three size ranges are shown in Figure 3 and essentially comprise the whole distribution of the atomized powder.

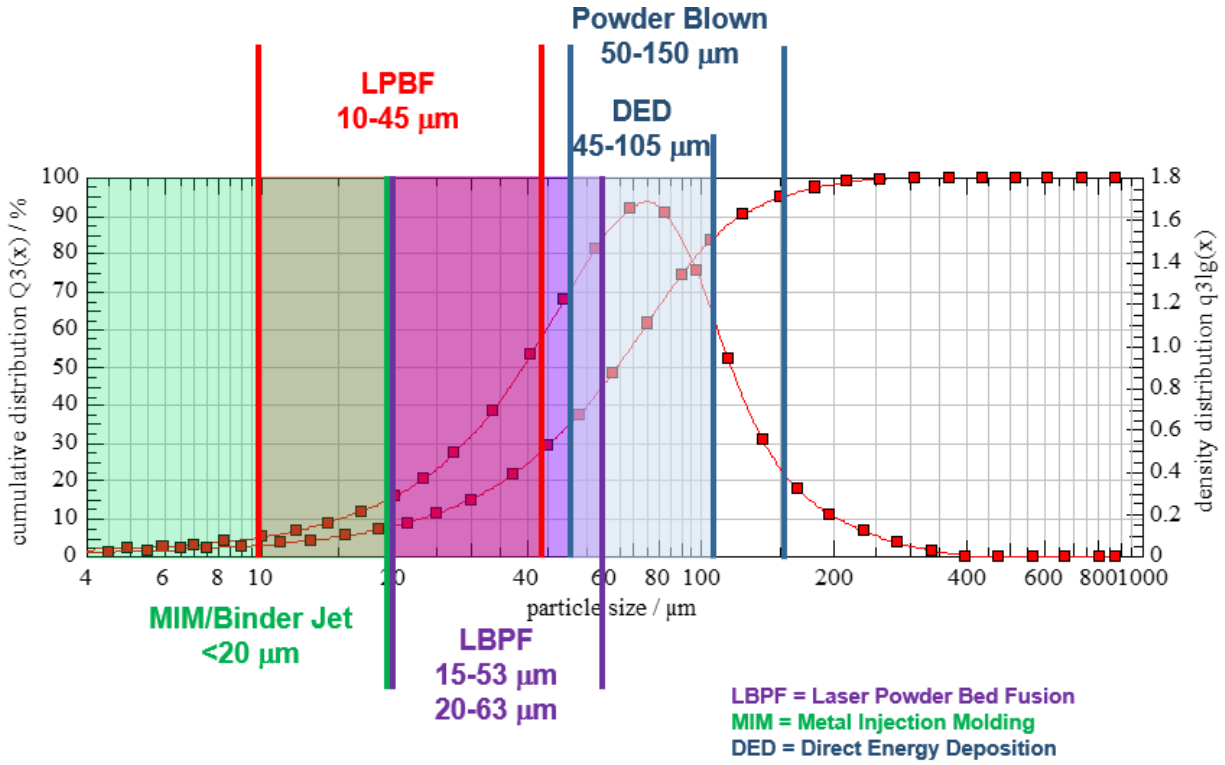

Figure 3: Plot of cumulative particle size for gas atomized powder showing particle size range for different AM processes.

The < 25-micron powder was printed on an ExOne Innovent Plus with a solvent binder, while the 15–53-micron powder was printed on an EOS M290 laser powder bed printer. Layer thickness for the ExOne binder jet printed parts was 50 microns and 40 microns for EOS laser printed parts. Test specimens for DED were produced using an Optomec MTS 500-CA DED system equipped with a 1 kW Ytterbium-doped fiber laser (IPG Photonics; $\lambda = 1070$ nm). The test samples for DED were printed using a particle size from 45-105 microns with a laser power of 498W, scan speed of 12 mm/s, hatch spacing of 0.4 mm, layer height of 0.6 mm, and a powder feed rate setting of 6 RPM. Powder properties for this study are listed in Table II.

Table II: Powder Properties

	Apparent Density	Tap Density	Carbon	Sulfur	Oxygen	Nitrogen	d_{10}	d_{50}	d_{90}	Carney Flow
Material	**g/cm³**	**g/cm³**	**wt.%**	**wt.%**	**wt.%**	**wt.%**	**Micrometers**	**Micrometers**	**Micrometers**	**Secs**
Ancor AM Iron < 25 Microns	4.35	4.98	0.006	0.004	0.05	0.001	6.1	14.5	24.6	1.8 C
Ancor AM Iron 15-53 Microns	4.35	4.90	0.002	0.003	0.03	0.001	21.6	33.6	49.5	13.5
Ancor AM Iron 45-105 Microns	4.52	4.80	0.005	0.004	0.02	0.001	39.6	61.9	93.2	2.9 C
Carbonyl SQ	2.41	4.26	0.015	0.0003	0.24	0.005	2.4	6.6	47.2	NF

Magnetic torroids nominally measuring outer diameter of 36 mm, inner diameter of 22 mm, and height of 6 mm were printed on all printers. Initial sintering for the binder jet samples was performed in an Abbott belt furnace with a preheat zone at 730°C and hot zone at 1260°C with ~ 20 minutes at temperature in a 100 v/o hydrogen atmosphere to remove the binder. A second sintering step was performed in a Solar Vacuum furnace at temperatures of 1360, 1380 and 1400°C and held for 2 hours under a partial pressure of hydrogen. In some cases, specimens were subjected to a post sintering heat treatment to increase the grain size. These experiments were performed in the Abbott belt furnace at 1150°C and 1260°C for 20 minutes at temperature in 100 v/o hydrogen atmosphere.

Five tensile specimens were evaluated for each print method. The densities of sintered steels were determined in accordance with MPIF Standard 42. Tensile testing followed MPIF Standard 10 and apparent hardness measurements were conducted on the tensile specimens, in accordance with MPIF Standard 43.

Porosity measurements were made on metallographically prepared cross-sections removed from test parts. A Clemex automated image analysis system was used to measure and map the porosity on as-prepared surfaces using a predetermined gray level to separate the dark void space and from the highly light reflective metallic regions. This provided the opportunity to estimate the pore content in both the sample volume and in localized regions.

Specimens for microstructural characterization were prepared using standard metallographic procedures. Subsequently, they were examined by light optical microscopy in the polished and etched (2 w/o nital / 4 w/o picral.) conditions.

Magnetic data was collected using SMT 700 measuring system from KJS associates using toroidal samples with 200primary and 40 secondary copper windings using #28AWG wire for DC measurements. DC hysteresis is traced using the procedure in the standards ASTM773(IEC 60404-4). For AC measurements, ASTM A927 procedure was used, typically with 200 primary turns and 40 secondary turns.

RESULTS AND DISCUSSION

Results of MBJ

One of the benefits of the gas atomized pure iron powder over carbonyl or fine powder derived from sponge iron is that the powder is slightly coarser and has better flowability, thus allowing it to be used with MBJ. Inherently, the sinter-ability of pure iron is extremely low, so in order to evaluate the magnetic response of the iron powder processed by binder jetting, the powder was mixed with 2.9% of Fe_3P to make an MPIF designated FY-4500 (commonly known as 45P), which is a soft magnetic alloy. Soft magnetic alloys are used in DC magnetic fields and are easily magnetized and de-magnetized. The Fe_3P addition forms a liquid phase, which enhances the alpha phase sintering response of the iron powder.

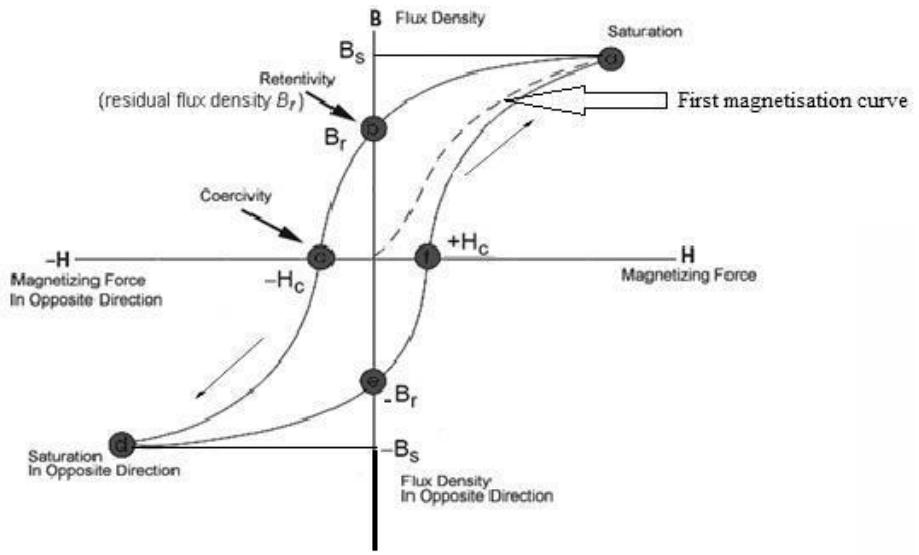

Figure 4: Hysteresis loop of ferromagnetic material, like Iron. [7]

In order to understand the key soft magnetic properties and terminology, a general magnetic hysteresis curve is presented in Figure 4. When a ferromagnetic material, such as iron, is exposed to the application of an external magnetic field (H), magnetic domains inside the ferromagnetic material will begin to align resulting in magnetic induction (B) as represented by the following equation, $B=H+4\pi M$. The ratio (slope) *B*/*H* is defined as the permeability, μ. This value indicates the relative increase in flux or magnetic induction caused by the presence of the applied magnetic field. The initial permeability, μ_0, and the maximum permeability, μ_{max}, are of the most importance for PM applications. The initial permeability, μ_0, is simply the slope of the initial portion of the magnetization curve, say to 0.01 T (100 G). The maximum permeability, μ_{max}, is the slope to the tangent of the magnetization curve. After μ_{max} is reached, the permeability falls off rapidly and eventually reaches a value of 0, where the material is considered fully magnetized, as all magnetic domains are now aligned in the same direction. At this point, the magnet is said to be saturated or has reached saturation induction (B_s). In other words, even though the magnetization curve will continue to show a slight increase due to increasing applied field H, the magnetic material does not contribute any additional induction. If the applied field is then removed (reduced to zero), the induction in the material is also reduced, but some induction will remain. This is considered the residual induction or remanence (B_r). In order to reduce the induction back to zero, a reverse applied field must be applied. The amount of reverse field necessary to return the induction to zero is referred to as the coercive force or coercivity (H_c). When the coercive force is applied, the magnetic domains will become sufficiently randomly oriented so that the material has a net magnetization of zero. In an alternating current (AC) application, the applied force is applied alternatively in the positive and negative directions at a given frequency, forcing the material to go around this hysteresis loop many times per second. The area inside the loop in AC applications is referred to as core losses, typically energy lost in the form of heat. It is for this reason that ideal soft magnetic materials will have high permeability and low coercivity, leading to low losses.

Impurities, such as carbon, nitrogen, and oxygen, even in the smallest amounts, lead to large decreases in magnetic performance. Soft magnetic materials, such as FY-4500, are used in a variety of applications including linear actuators, solenoids, and transformer cores.[8-12] These applications require high magnetic permeability, high magnetic flux density, and low coercive force. To achieve these excellent magnetic properties, impurity levels need to remain low. The effect of carbon on magnetic properties is well known, in which carbon amounts greater than even 0.01% will increase coercivity and decrease magnetic permeability. The atomized powder used in the MBJ process (shown in Table II) has lower

residual content than in normal powders used in press and sinter applications. Table III shows the magnetic properties obtained from the hysteresis curve of the MBJ FY-4500 material versus the MPIF standard values for soft magnetic materials and an actual FY-4500 produced by conventional PM. [13] In relation to density, the fine particle size used in MBJ FY-4500 (<25 microns) and the high sintering temperature (1380 ^{o}C) led to a 7.42 g/cm^3 density, allowing for direct comparison of the magnetic properties with the standard materials. When looking at the coercivity (H_c) of the various materials in Table III, the MBJ material has the lowest value of any of the processed FY-4500 samples and approaches that of the FN-5000 (50% nickel bearing grade). Since the coercivity is the amount of magnetizing field necessary to demagnetize the material, the MBJ FY-4500 material would be useful in applications such as solenoids or switching circuits. Since the impurities in the powder utilized in the MBJ FY-4500 are extremely low, the maximum permeability is higher than any of the other materials listed in Table III. The maximum induction (B_{max}) is a measure of the magnetization the material can achieve at a given applied field and the MBJ FY-4500 again out-performs the FN-5000, nickel bearing material leading to potentially significant cost savings.

Table III: Magnetic Property Comparison MBJ to MPIF Standard Materials and Typical PM.

Sample	Density (g/cm^3)	μ_{max}	Bmax @ 15 Oe (G)	Hc @ 15 Oe (Oe)
FF-0000 MPIF STD (Iron)	7.2	2,900	12,000	1.8
FY-4500 MPIF STD (Phosphorus)	7.4	3,600	13,500	1.5
FS-0300 MPIF STD (Silicon)	7.4	6,000	14,000	0.9
FN-5000 MPIF STD (Nickel)	7.5	10,000	12,000	0.3
FY-4500 Produced via PM (Phosphorus)	7.20	3,984	11,850	1.42
FY-4500 Produced via MBJ (Phosphorus)	7.42	17,732	16,485	0.46

One advantage of the sintering process used in binder jetting is that it can be done in a reducing atmosphere (such as hydrogen) and, additionally, under vacuum. This can lead to a reduction in the oxygen and nitrogen levels. The high sintering temperatures utilized with these atmospheres also are a benefit as they lead to grain growth and less grain boundary area. Figure 5 shows the porosity level and grain size of the MBJ FY-4500. The porosity is rounded and isolated, limiting surface area. The grain size of the material is several hundred microns, most likely due to the lack of any residuals to impede grain growth and also due to the high sintering temperature (1380 ^{o}C).

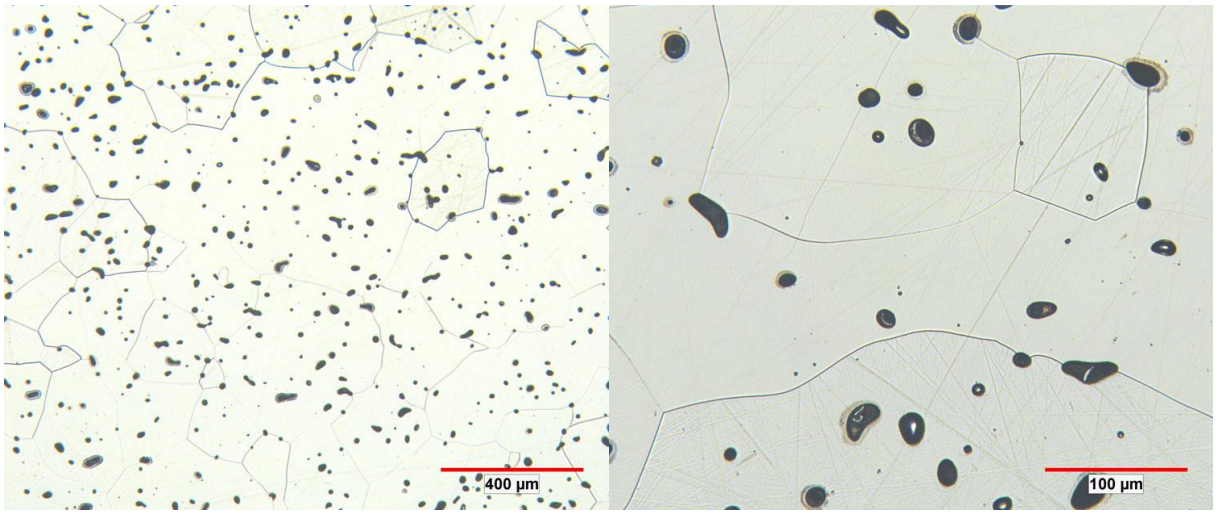

Figure 5: Etched microstructure of MBJ pure iron. (Etch 2% Nital / 4% Picral) Density = 94.9%

While mechanical properties are generally not the main design feature for magnetic materials, soft magnetic parts are used in a wide range of applications working in different environmental conditions. Changes in mechanical properties in relation to service temperature have to be considered. Table IV lists room temperature tensile properties and hardness of the MBJ printed FY-4500 versus those contained in the MPIF standard. The tensile properties exceed that of the material produced by conventional press and sinter techniques, while the hardness is slightly lower. The lower hardness could be contributed to a larger grain size in the MBJ material.

Table IV: Mechanical Properties of FY-4500 produced by MBJ and LPBF versus MPIF Standards

Material	Density (g/cm^3)	UTS (MPa)	YS (MPa)	Elongation (%)	Apparent Hardness
FF-0000-20X MPIF STD (Iron)	7.1	255	155	17	55 HRF
FY-4500-17Y MPIF STD (Phosphorus)	7.3	415	280	15	65 HRB
FS-0300-11Y MPIF STD (Silicon)	7.4	415	310	20	80 HRB
FN-5000-5Z MPIF STD (Nickel)	7.4	275	170	15	40 HRB
FY-4500 Produced via LPBF (Phosphorus)	7.68	428	375	30	72 HRB
FY-4500 Produced via MBJ (Phosphorus)	7.42	453	285	27	60 HRB

Results of LBPF

In the case of LBPF (Laser Powder Bed Fusion), the magnetic properties can be compared directly to wrought materials because the material is melted layer-by-layer to produce a nearly 100% dense

specimen. Therefore, the pure iron could be tested as opposed to a FY-4500 necessary in the case of MBJ (due to the poor sinterability of pure iron). Since the laser melting process takes place under argon, there is virtually no pick-up of residual nitrogen or oxygen, which are both detrimental to magnetic properties. The typical microstructure of the LPBF printed samples is ferritic with large columnar grains that follow the heat flow from the laser. However, even though the material is single phase ferrite, the transformation from austenite to ferrite during the cooling process leads to a residual stress from the phase transformation. Commercial grade soft magnetic materials processed by PM route are listed Table V. The permeability of the LPBF samples increases with heat treatments to remove the residual stress from the transformation of austenite to ferrite that takes place when the melt pool cools from the liquid to room temperature iron. Since the annealing was done under a partial pressure of hydrogen, reduction occurs of other impurities such as carbon, oxygen, nitrogen and, under the right conditions, sulfur. While not optimized for this study, hydrogen annealing lowers the coercive force and improves maximum relative permeability. This is shown in Table V, as the maximum permeability increased, and the coercive force decreased with an increase in temperature of annealing.

Table V: Magnetic Properties of LPBF Samples versus MPIF and Pure Iron

Process	Coercive force H_c A/m	Permeability μ_{max}	Saturation Induction, T @10000A/m(125Oe)	Density g/cm^3
LPBF As Printed	244	1293	1.87	7.76
1120 ^{0}C annealed H2,slow cooled	110	3337	1.82	7.71
1260 ^{0}C annealed ,H2, slow cooled	95	4922	1.8	7.71
FF-0000-20X	160	2900	1.2	7.1
Ingot (99.8% Fe)	112	1000	2.15	NA
Commercially Pure Fe	20-100	3500-20,000	2.15	NA

The coercive force of the annealed materials also depends on grain size. Annealing increases the grain size and also contributes to the lowering of coercive force. The size and shapes of the pores can also contribute, but the porosity in the LPBF samples is low, and the pores are well-rounded, minimizing the surface area. The etched microstructures of the LPBF samples of pure iron are shown in Figure 6.

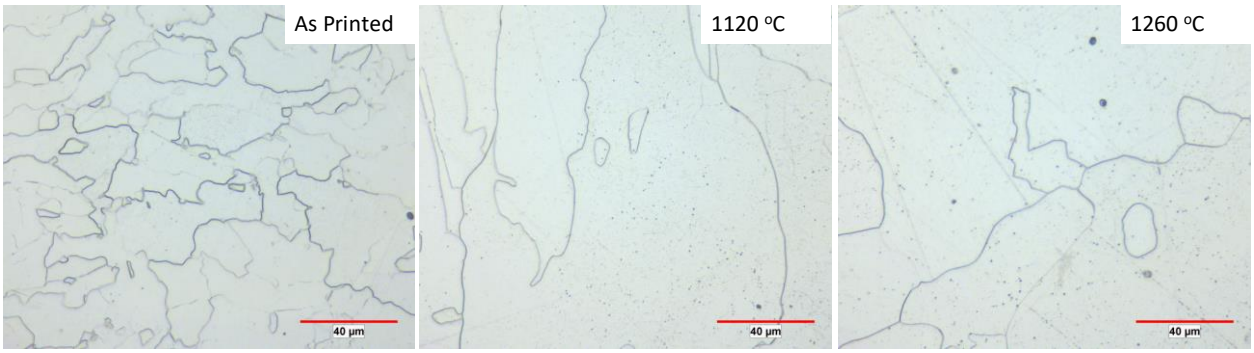

Figure 6: Etched microstructure of LPBF printed pure iron. (Etch 2% Nital / 4% Picral) Density = 99.5%

Results of Direct Energy Deposition (DED)

The DED process utilizes the 45–105-micron powder size distribution. During the atomization process, residuals, particularly the interstitial elements like carbon and oxygen, tend to segregate to the finer particles of the size distribution. Additionally, the surface area of this size distribution is less than that used for MBJ or LPBF. As shown in Table II, the DED powder (45-105 Microns) has the lowest oxygen content of any of the powders utilized in this study. In addition, since the scan rate of DED is much slower than that of LPBF the heat input would be much higher in the DED process. This would lead to a much slower rate of solidification and cooling, and it has been found that the grains are much coarser in DED printed material than LBPF.[14]

Table VI: Magnetic Properties of LPBF Samples versus DED and Pure Iron

Process	Coercive force H_c A/m	Permeability μ_{max}	Saturation Induction, T @10000A/m(125Oe)
LPBF As Printed	244	1293	1.87
DED As Printed	102	2669	1.76
LPBF 1120 ^{0} C annealed H2-slow cooled	110	3337	1.82
DED 1120 ^{0} C annealed H2-slow cooled	87	3958	1.75
LPBF 1260 ^{0} C annealed H2-slow cooled	95	4922	1.80
DED 1260 ^{0} C annealed H2-slow cooled	71	5720	1.7
FF-0000-20X	160	2900	1.2
Ingot (99.8% Fe)	112	1000	2.15
Commercially Pure Fe	20-100	3500-20,000	2.15

The porosity of the DED samples was measured by image analysis and was determined to be approximately 0.50% (measure on an area basis), which matches very closely to the porosity measured in the powder itself. The conventional theory is that whatever porosity exists in the powder as it is atomized remains in the as-printed structure. The porosity measured in the LPBF powder (15-53 microns) was only 0.22%. Despite the fact that the DED-produced pure iron had a higher porosity level, the printed samples had a lower coercivity and higher permeability than the samples produced from LPBF. The grain size of the DED samples is shown in Figure 7. The larger grains and the higher purity (lower interstitials) of the DED produced samples appear to overcome the slightly higher levels of porosity in the powder when compared to LPBF in both the as printed condition and annealed at 1120 and 1260ºC.

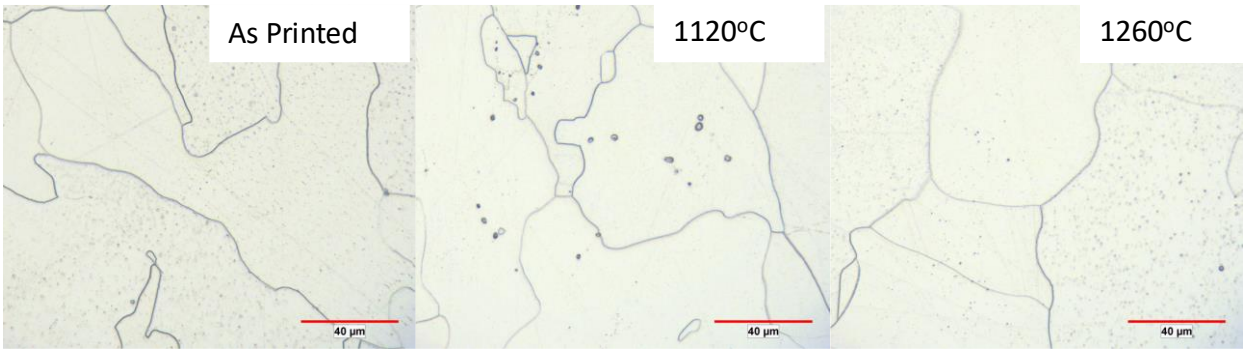

Figure 7: Etched microstructure of DED printed pure iron. (Etch 2% Nital / 4% Picral) Density = 99.5%

Table VI shows that the coercive force is lower, and the maximum permeability is higher for the DED samples versus the LPBF processed under the same conditions. These are both desirable outcomes that appear directly related to the increase in grain size produced by the DED processing.

CONCLUSIONS

The purity of the iron powder produced by the EIGA process in combination with very high purity feedstock has led to improvements in magnetic properties that cannot be achieved by conventional iron powder making processes. While exclusively used in additive manufacturing processes for magnetic applications in this work, the implications are that the enhanced purity will be useful in other applications that include catalysts, water remediation and, most importantly, energy storage such as batteries. These applications will be examined in future work.

REFERENCES

1. R. D. McKerracher, C.Ponce de Leon, R. G. A. Wills, A. A. Shah, and F.C. Walsh, " A Review of the Iron-Air Secondary Battery for Energy Storage," ChemPlusChem 2015,80, pp. 323 – 335.
2. A. K. Manohar,S. Malkhandi, B.Yang, C.Yang, G. K. Surya Prakash, and S. R. Narayanan, "A High-Performance Rechargeable Iron Electrode for Large-Scale Battery-Based Energy Storage," Journal of The Electrochemical Society, 159 (8) pp. A1209-A1214, (2012).
3. P. Periasamy, B. Ramesh Bahu, S. Venkatakrishna Iyer, "Performance characterization of sintered iron electrodes in nickel/iron alkaline batteries," Journal of Power Sources, 62, (1996) pp. 9-14.
4. T. Bigg and S.J. Judd, "Zero Valent Iron for Water Treatment," Environmental Technology, Vol.21, pp.661-670, 2000.
5. K.S. Sista, D. Kumar,G.R. Sinha, A.P.Moon and S. Dwarapudi, "Iron Powders as a Potential Material for Arsenic Removal in Aqueous Systems," ISIJ International, Vol. 61 (2021), No. 11, pp. 2687–2702.
6. T. Klein and D. Knorr, "Oxygen Adsorption Properties of Iron Powder," Journal of Food Science, 1990, Vol.55, No.3, pp.869-870.
7. G.S. Yadav, D.K. Dey, Ganpati, A.Kumari and T.K. Dey, "Application of Ferrite Medium in Microwave Devices," (ISTAM), Proceedings of 60th Congress of ISTAM, MNIT, Jaipur, Rajasthan, India, Dec. 16-19, 2015, Section, SM8.

8. K. Narasimhan, M. Marucci and C. Schade "Advancements in Insulated Powder Composites for Soft Magnetic Applications," *Advances in Powder Metallurgy and Particulate Materials – 2012*, compiled by I. Donaldson and N. Mares, Metal Powder Industries Federation, Princeton, NJ, 2012, part 10 pp.113-120.

9. K. Narasimhan and C. Schade "Iron-Silicon Water Atomized for Electromagnetic Applications," *Advances in Powder Metallurgy and Particulate Materials – 2014*, compiled by R. Chernekoff and W.B. James, Metal Powder Industries Federation, Princeton, NJ, 2014, part 10 pp.223-233.

10. K. Narasimhan, "Powder Metallurgy Routes to Make Parts for Magnetic Applications," *Advances in Powder Metallurgy and Particulate Materials – 2016*, compiled by C. Blais and J. Hamilton, Metal Powder Industries Federation, Princeton, NJ, 2016, pp.768-782.

11. C.G. Oliver and H.G. Rutz, "Powder Metallurgy in Electronic Applications," *Advances in Powder Metallurgy and Particulate Materials*, Metal Powder Industries Federation, Princeton, NJ, 2016, Vol. 3, part 11, pp. 87-102.

12. M. Marucci and K. Narasimhan, "Advancements in Insulated Powder Composites for Soft Magnetic Applications", Proceedings of the European PM Conference, 2011, Vol. 1. Page 291.

13. MPIF Standards for Structural Parts 35, Metal Powder Industries Federation, Princeton, NJ.

14. M. Ma, Z.Wang and X. Zeng, "A Comparison on Metallurgical Behaviors of 316L Stainless Steel by Selective Laser Melting and Laser Cladding Deposition," Materials Science and Engineering A, 2017, 685, pp.265-273.